*J Mater Sci: Mater Electron* (2022) 33:15574–15585

# Synthesis and characterization of different graphite/chitosan ink ratio composition towards flexible strain sensor performance

Nur Iffah Irdina Maizal Hairi[1], Aliza Aini Md Ralib[1,*], Farah B. Ahmad[3], and Maziati Akmal bt Mat Hattar[2]

[1] *Department of Electrical and Computer Engineering, Kulliyyah of Engineering, International Islamic University, Malaysia, Kuala Lumpur, Malaysia*
[2] *Department of Science Engineering, Kulliyyah of Engineering, International Islamic University, Malaysia, Kuala Lumpur, Malaysia*
[3] *Department of Biotechnology Engineering, Kulliyyah of Engineering, International Islamic University, Malaysia, Kuala Lumpur, Malaysia*

**Received:** 30 January 2022
**Accepted:** 21 May 2022
**Published online:** 7 June 2022



## ABSTRACT

Flexible and stretchable strain sensors are getting vast attention to be implied in various wearable devices application. However, most conventional strain sensor is having limitations in achieving both high stretchability and sensitivity. Selection of materials for conductive fillers and binders are crucial in producing the stretchable ink for strain sensors. Biopolymer materials such as chitosan started to be implied in various application such as gas sensor and electrochemical sensor. Chitosan has advantages to be a good binder as it exerts significant physical properties. Conductive fillers such as graphite powder are known to be having good electrical conductivity. Hence, this paper aims to investigate the effect of different graphite/chitosan ink ratio composition towards flexible and stretchable strain sensor performance. Three different graphite/chitosan ink ratios of 1:2, 1:3, and 1:4 were synthesized. The surface morphology shows that the graphite/chitosan ink ratio 1:2 has the most compact structure resulting to good adaptability, conductivity, and flexibility. The XRD and FTIR results illustrate that graphite are successfully synthesized with chitosan solution. Measurement result shows that the highest strain detection range is also attainable by graphite/chitosan ink ratio of 1:2 at 83.3% strain and gauge factor of 5.44. This concludes that graphite/chitosan ink ratio of 1:2 is the optimum ratio as highest stretchability and sensitivity are recorded. Therefore, it is important to have an adequate amount of chitosan solution to obtain good ink structure and great performance of strain sensor.

Address correspondence to E-mail: alizaaini@iium.edu.my


https://doi.org/10.1007/s10854-022-08463-8

## 1 Introduction

Recently, electronic sensing devices have been receiving numerous developments of strain sensors as it has wide applications such as the magnetic applications [1], medical diagnostic, environmental monitoring [2], and wearable electronics [3]. Various strain-sensing mechanism which includes capacitive sensing [4] and piezoresistive sensing [5] have been developed to fabricate a highly sensitive strain sensor. Although much progress for strain sensors has been made in multiple areas, some of the reported flexible strain sensor still having some limitations. Most conventional strain sensors are only able to provide high sensitivity but not high stretchability due to the usage of metals in the strain sensor fabrication [6, 7]. In addition, the fabrication of existing strain sensor is costly as it undergoes complicated process and equipment [8]. Tang et al. [9] stated that the presence of sensitive devices such as scanning electron microscopies are able to measure up to nm-scale resolution. However, it is still incapable to measure the details of a plant growth as it can only detect small samples, not the elongation and physical growth of the plants. In addition, it also required destructive pre-treatment process which is complicated and time consuming [9]. Therefore, there is a need to integrate new materials in fabricating strain sensor to produce highly sensitive and stretchable sensors that require simple process without sample pre-treatment, reduce time and capable of having both sensitivity and wide range of strain detection.

Generally, there are two different components in printed strain sensor which are the substrate layer and the printing ink [10]. The substrate acts as the base layer and plays an important role as it determines the stretchability, bendability, printability, and durability of the sensor. Meanwhile, filler and binder are among two main components that will affect the capability of the strain sensor upon multiple bending and flexing [10]. Fillers act as the active component which describe the properties and features required for printing ink, while binder is used to bind the ink particles together to assist the binding mechanism of the printed trace and allow homogenous dispersion of the ink. Carbon-based materials are one of common metallic component to be used as fillers such as graphene [11, 12], graphite [8], carbon black [13, 14], and silver [7, 15]. On the other hand, styrene [16], silicone [17], and urethane [14, 18] are among several resins that are used in binders in flexible sensors fabrication.

Recently, the integration of chitosan as binder in strain sensor fabrication has started to attract vast attention among researchers. Chitosan is a biopolymer, produced by alkali deacetylation of chitin obtained from exoskeletons of edible marine crustaceans such as shrimps and crabs. It exerts significant physical properties that provide antioxidant [19], great biocompatibility [20, 21], biodegradability [21], and environmental friendly [2, 21]. Ayad et al. [22] fabricated a gas sensor by utilizing chitosan solution to be dropped casted onto the Quartz Crystal Microbalance (QCM) electrode to observe the kinetics of methylamine adsorption. The integration of chitosan solution in this experiment resulted to the highest diffusion coefficient value obtained by methylamine compared to dimethylamine and diethylamine [22]. Besides, Balyan et al. [21] successfully utilized chitosan film as energy harvesting properties by converting water vapor into electrical energy.

In this work, chitosan solution will be integrated with graphite powder as the binder. The presence of chitosan resulted in a non-breakable ink content which makes the adherence between both substrate and layered element (ink) stronger. Due to the tensile strength of chitosan, it can withstand various deformation of stress and strain applied to them. This will avoid the sensor to delicate when any bending or stretching occurs. In addition, homogenous dispersion of ink can be obtained. This resulted to wider strain detection range which means higher stretchability will be achieved. Hence, this paper aims to investigate the effect of different graphite/chitosan ink ratio composition towards flexible and stretchable strain sensor. The characterization of graphite/chitosan ink mixture and the measurement of the electrical properties of the graphite/chitosan ink ratio will be evaluated. The materials and methodology used in this work were discussed in Sect. 3. Meanwhile, Sect. 4 focuses on analyzing the materials characterization that covers the XRD, SEM, FTIR, and Raman spectrum. The performance of the chitosan-based strain sensor was also explained and portrayed in Sect. 4 in terms of their sensitivity and stretchability. Finally, the conclusion is presented in Sect. 5.

## 2 Experimental section

### 2.1 Materials and methods

Briefly, the preparation of the ink started by diluting 0.58 mL acetic acid to 100 mL water. This solution is then used to dissolve the chitosan (1 g). The chitosan-based ink was synthesized by mixing the graphite powder and the CS with a ratio of 1:2 (w:v). The graphite powder used in this experiment is ≤ 20 µm in size. The mixture between graphite and CS is stirred for 1 min before obtaining a chitosan–graphite ink. The fabrication process of the chitosan-based strain sensor is illustrated in Fig. 1.

The characterization of graphite/chitosan ink mixture was conducted using FTIR (NicoletTM iS50 FTIR, ThermoFisher Scientific, Massachusetts, United States) with spectral ranges from 4000 to 400 $cm^{-1}$ resolution with 20 scans. Surface morphology of graphite/chitosan ink was captured by using FESEM JEOL JSM-7800F operating at 7 kV. The molecular structure for graphite/chitosan ink mixture was identified using XRD DSC-60 Plus. Raman spectra of graphite/chitosan ink were studied using the Renishaw1000 micro-Raman spectrometer by using excitation wavelength of 785 nm.

Due to the good viscosity of the graphite–chitosan ink fabricated, the toothpick technique is used in fabricating the strain sensor. A latex glove was cut into approximately 6 cm to occupy the inks that are to be swabbed. Next, a toothpick was used to dip into the ink and written onto the latex glove. This ink was then spread accordingly and cure in a room temperature for ≈ 5 min. The setup is shown in Fig. 2a.

As the conductivity of the chitosan–graphite ink is crucial for the strain sensor to function properly, conductivity test is conducted by writing a simple circuit demonstrated in Fig. 2b. The graphite/chitosan ink is written onto a glass slide and connected to the LED. The same steps are repeated for all ink ratios for the conductivity test. This circuit was then connected to the power source and a light from the LED was observed accordingly.

The changes in resistance of the written graphite/chitosan ink upon curing at room temperature on different ink composition were evaluated. A measurement setup as shown in Fig. 2c was conducted. Firstly, the latex glove was cut for approximately 5 cm and the graphite/chitosan ink with ratio 1:2 was written onto it using the toothpick. Next, two copper wires are attached to each end of the ink and taped to the table to secure its position. The copper wires were then clipped with the crocodile clip connected to the handheld multimeter to monitor the resistance reading. The initial resistance recorded was considered at time = 0 min. The resistance reading will be taken continuously for every 3 min until a constant reading of resistance was obtained. By having a constant reading at a particular time, the conductivity of the three ink ratios can also be

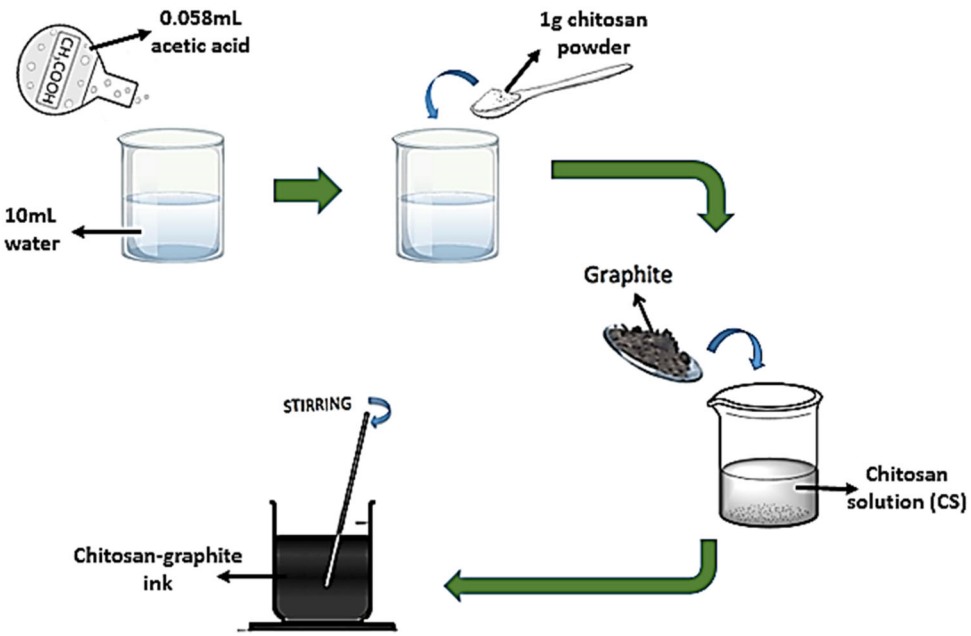


**Fig. 1** Preparation of graphite/chitosan ink

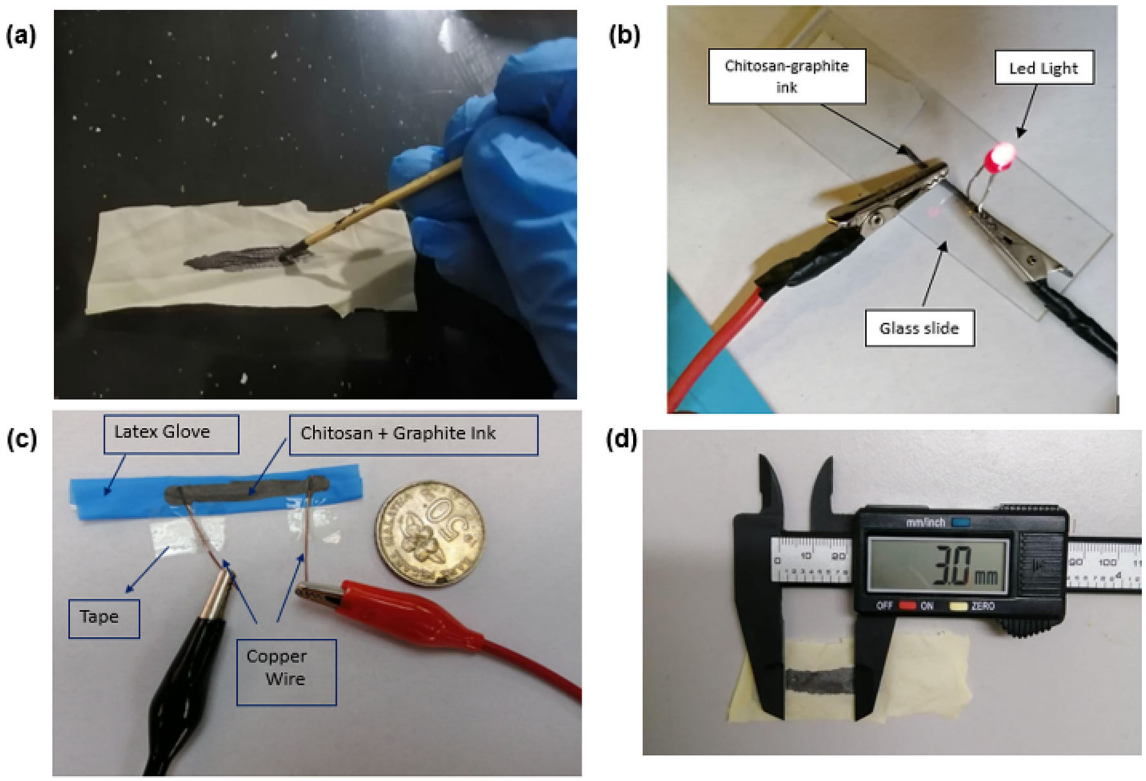


**Fig. 2** **a** Toothpick technique used in fabricating the strain sensor. **b** Simple circuit diagram for ink conductivity test using LED light. **c** Experiment setup for resistance changes test of written ink upon curing at room temperature. **d** Stretchability test setup

evaluated. The same procedure was repeated for the graphite–chitosan ink having ink ratios of 1:3 and 1:4.

Stretchability test is crucial in determining the performance of the fabricated chitosan–graphite strain sensor. Figure 2d shows the experiment setup for the strain sensor in observing its stretchability performance. The stretchability is measured by measuring the changes of resistance as the inks are stretched. The ink was swab for 3.0 mm onto the latex glove and attached to the electronic digital caliper to measure its length. The strain sensor will be stretched for 0.2 mm until maximum attainable strain is observed. All three ratios of chitosan and graphite mixture were tested in this experiment using the same experiment setup.

Next, the sensitivity of the fabricated strain sensor was investigated as it is one of the crucial parameters to determine the sensor's performance. The sensitivity of the strain sensor is represented by the gauge factor (GF), having the ratio of relative changes in resistance ($\Delta R/R_0$) to the strain applied ($\varepsilon$). In this work, GF can be defined as the ratio of relative changes in resistance, to the mechanical strain applied. This can be mathematically expressed as

$$\mathrm{GF} = \frac{\Delta R/R_0}{\varepsilon}. \quad (1)$$

Lastly, the adaptability of the sensor is observed to ensure the sensor can adapt to various deformation on substrate such as bending [8]. The mixture of graphite and chitosan ink was mixed and written onto the latex glove using toothpick. The bending of the sensor is then evaluated by bending and relaxing the sensor for three times. The same steps are repeated for all three ratios of the chitosan–graphite ink.

## 3 Results and discussion

### 3.1 Material characterization

Figure 3 shows the SEM image of graphite/chitosan ink ratio composition of 1:2, 1:3, and 1:4. These three samples were tested to observe the external morphology and the chemical composition of the ink having different mixtures of chitosan solution and graphite powder. Based on the SEM images obtained, graphite/chitosan ink with ratio of 1:2 (Fig. 3a) has

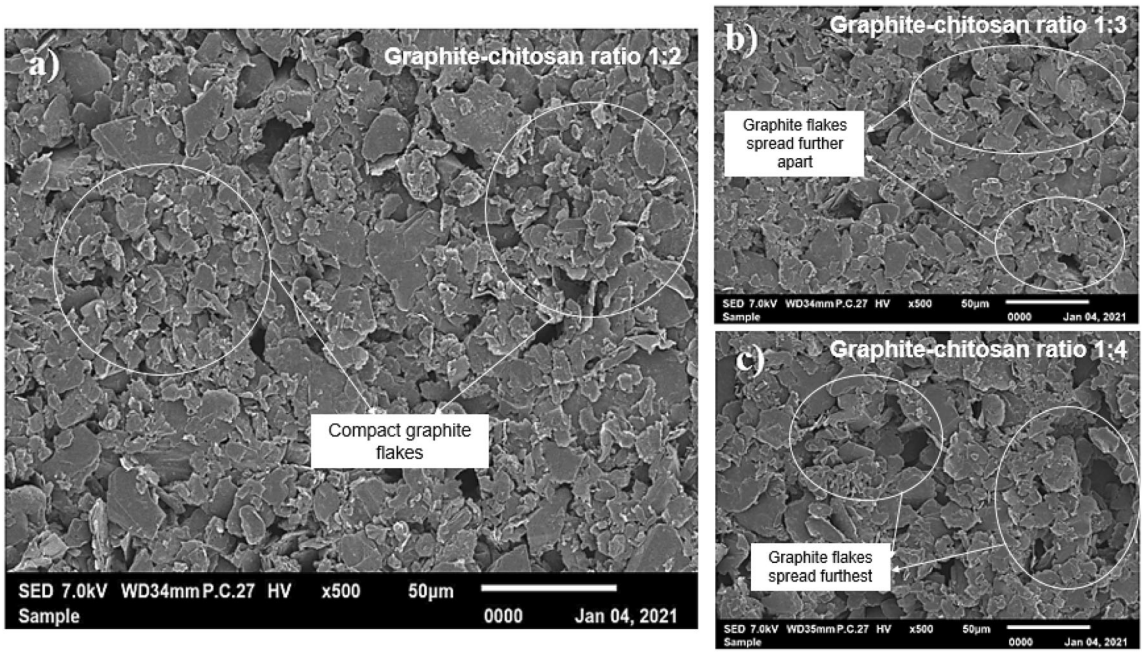


**Fig. 3** SEM images. **a** Graphite/chitosan ink of ratio 1:2. **b** Graphite/chitosan ink of ratio 1:3. **c** Graphite/chitosan ink of ratio 1:4

the most compact structure compared to the ink with ratios of 1:3 (Fig. 3b) and 1:4 (Fig. 3c). The graphite flakes of 1:2 are closer to each other resulting in high adhesion and will increase the conductivity of the ink as compact particles will make the free electrons flow easily. For SEM images of graphite/chitosan ink with ratio 1:3, the graphite flakes are farther apart from each other and less compact compared to 1:2 while the ink with ratio 1:4 flakes are the farthest. This is because when the volume of the chitosan increases, it will change the morphology structure of the ink. The excessive volume of chitosan solution in the mixture of 1:3 and 1:4 will result in the graphite particles to spread further from each other as there is inadequate amount of graphite powder for the chitosan solution to bind. Therefore, graphite/chitosan ink with ratio 1:2 has the best adhesion and the most conductive ink contrast to graphite/chitosan with ratios 1:3 and 1:4 due to its compact and dense structure.

Figure 4 depicts XRD diffractogram for chitosan powder performed in the range of 5–80°. The first two major peaks appeared at $2\theta = 10.13°$ and 19.67° symbolizing the semi-crystalline structure of the chitosan. This result is in line with Yen et al. [23] as the characteristic peak of the normal chitosan observed to be in the range of 9–10° and 19–20° in order for the chitosan to have its crystallinity nature [23]. Besides, the XRD pattern for graphite powder and all three ratios for the graphite and chitosan mixture are also shown in Fig. 4. Firstly, the XRD pattern for graphite powder was analyzed. A major peak of $2\theta = 26.48°$ was observed. The diffraction of the graphite powder obtained in this project is well agreed with the standard reference of ICDD 00-008-0415 having the graphite peak at $2\theta = 26.42°$ showing its crystalline structure [24]. Following the XRD pattern of graphite powder is the XRD profiler for the mixture of graphite and chitosan solution. Having an additional substance which is the chitosan solution mixed with the graphite powder, a new or additional peak is expected to be observed in the XRD profiler regardless the volume of the chitosan solution added. As shown in Fig. 4, the additional peak expected for chitosan is absent. It is worth noting that the Bragg Brentano configuration of the XRD setup used for the graphite and chitosan ink mixture generally produces weak signal from chitosan due to its semi-crystalline nature while the graphite has a crystalline structure. Therefore, a broader peak was produced while the intense signal of the highly crystalline structure of graphite was observed [25].

Figure 5 shows the FTIR result for chitosan powder and the mixture of graphite/chitosan with ink ratio of 1:2. A broad absorption band at 3243.44 $cm^{-1}$ proves the presence of functional group –OH (H-bonded). Besides, the band at 2882.85 $cm^{-1}$ is

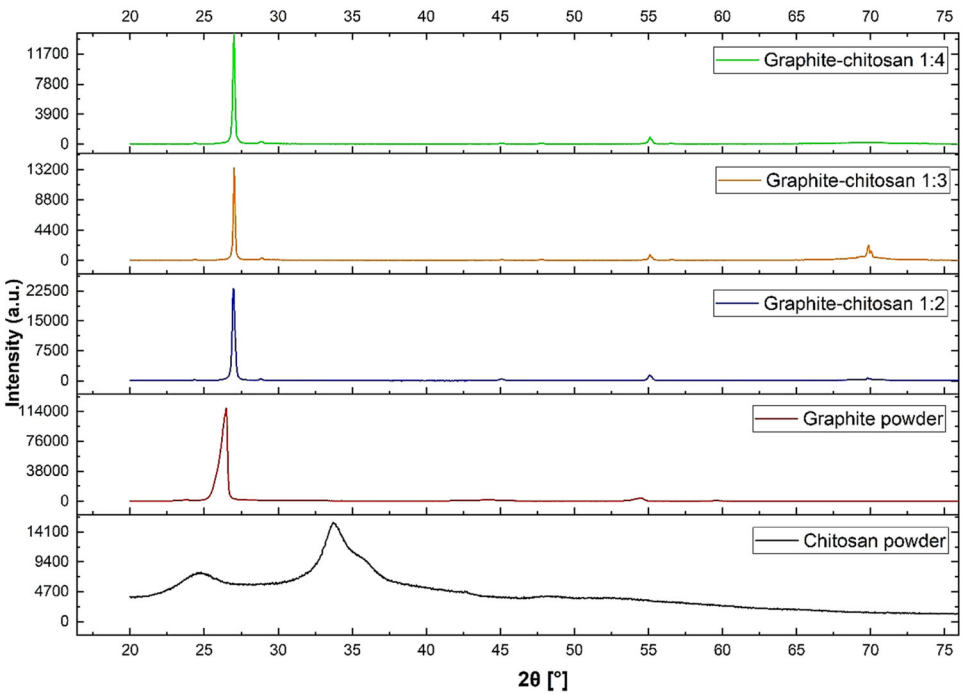


**Fig. 4** XRD profiler for chitosan powder, graphite powder, and three ratios of graphite/chitosan ink

attributed to the occurrence of the N–H stretching as shown in Fig. 5a. While, a vibrational mode of C=O stretching is observed at 1633.94 $cm^{-1}$ demonstrating the presence of a mid-band in the fabricated chitosan ink. Plus, the C–O stretching group which is also one of the major components of chitosan is represented by the peak at 1035.35 $cm^{-1}$ shown in the FTIR spectra. Once the graphite powder was added and mixed with the chitosan ink, peak shifting is observed in the FTIR spectra as shown in Fig. 5b. It is observed that the absorption band of –OH group for the mixture shifted from 3243.44 to 3243.25 $cm^{-1}$ and the N–H stretching band also shifted to 2881.66 $cm^{-1}$ compared to 2882.85 $cm^{-1}$ in chitosan solution. This is because the light absorbance will change once new materials are added into the chitosan solution resulting in shifting of the absorbance band.

Figure 6 demonstrates the Raman spectrum of graphite/chitosan ink ratio 1:2 performed using excitation wavelength of 785 nm. Two characteristic peaks were observed in the graphite/chitosan composite which are the D band and the G band. The D band is related to the disordered structure that results from the structural defects of the $sp^2$ atoms of graphite [26]. Meanwhile, the G band is caused by the in-plane stretching action between the $sp^2$ carbon atoms which relates to the in-phase $E_{2g}$ vibrational mode of the graphite lattice [26, 27]. The Raman spectra illustrate the presence of the D band centered at 1329 $cm^{-1}$ and the G band centered at 1579 $cm^{-1}$. This proved that although chitosan solution was added into the graphite, the bond of the graphite within the composite is not disrupted. This can be supported by the XRD results shown below where there is no secondary phase observed to indicate any presence of new structure developed within the graphite/chitosan composite.

## 3.2 Performance of sensor

The resistance effect can be observed based on Fig. 7. It is observed that the written graphite/chitosan ink for all ratios experienced a sharp decrease of resistance as soon as the ink was deposited on the substrate. This is due to the evaporation of water from the ink causing the ink to become totally harden at ≈ 50 kΩ for the first 3 min for all three ink ratios. The resistance continued to decrease until it reached ≈530 Ω on the 18 min for ink ratio 1:2, ≈ 550 Ω on the 18 min for ink ratio 1:3, and ≈ 1.16 kΩ on the 21 min for ink ratio 1:4. Once the inks reach these values, the resistance demonstrates a constant pattern as the value maintained at those levels for the next 3 min. It can be agreed that the graphite–chitosan ink ratio of 1:2 has the lowest resistance while the ink ratio of 1:4 has the highest resistance among the three

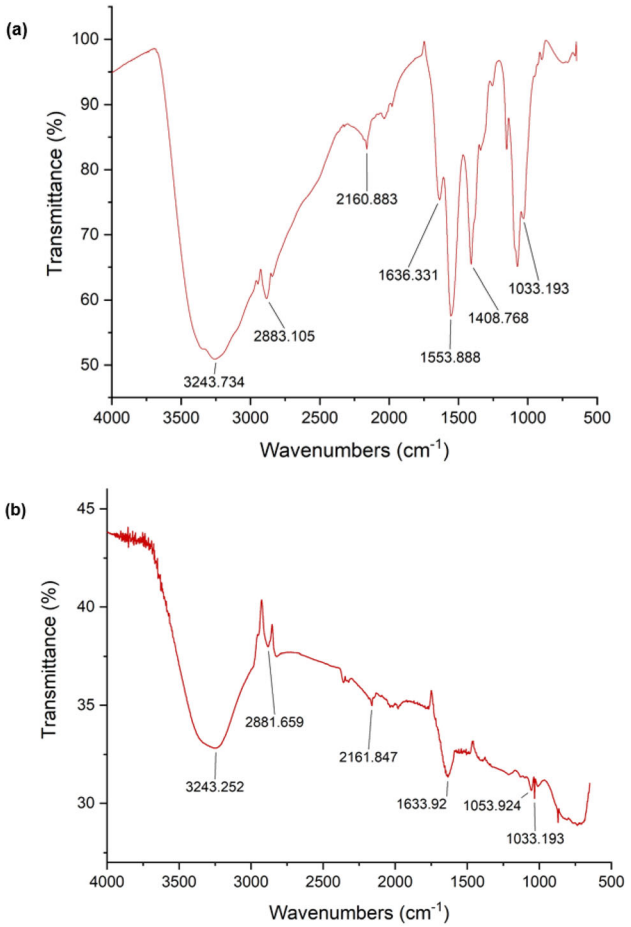


**Fig. 5** FTIR profiler. **a** Chitosan. **b** Mixture of graphite/chitosan ink ratio of 1:2

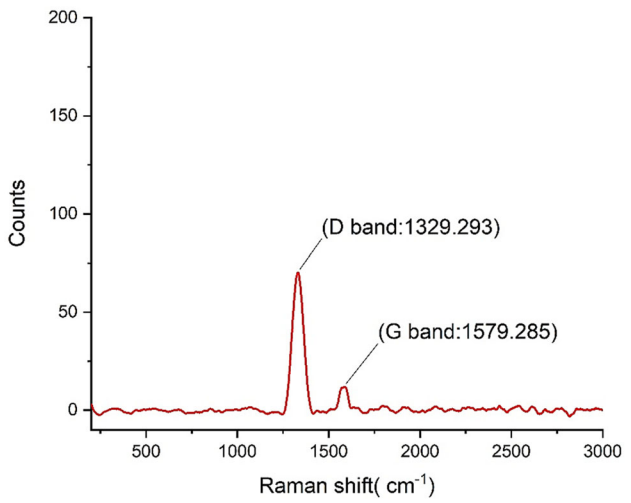


**Fig. 6** Raman spectra of graphite/chitosan mixture ink ratio of 1:2

ink ratios. This suggests that the excessive volume of binder in the ink ratio 1:4 will affect the resistance and the low viscosity of the ink is not suitable to write

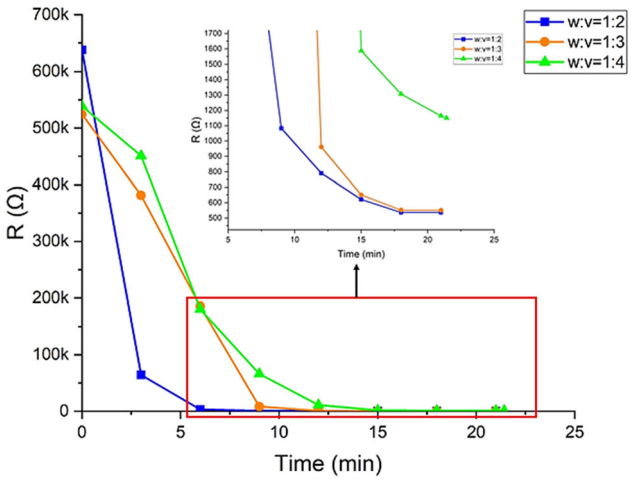


**Fig. 7** Resistance changes of graphite/chitosan ink upon curing at room temperature

a uniform membrane as it takes longer time to completely dry and harden. Meanwhile, the sufficient volume of binder mixed with the graphite powder for ink ratio 1:2 proves the best conductivity as it has the lowest resistance value recorded.

The relationship between the strain and changes of resistance ($\Delta R/R_0$) were measured for three different graphite/chitosan ink ratios (1:2, 1:3, and 1:4). The $\Delta R/R_0$ will determine the maximum strain that the strain sensor is able to withstand. The response of the sensor is observed to be linear under slight strain but started to have a drastic increase as the amount of the strain applied increases. Figure 8 shows the relative changes in resistance with respect to attainable strain

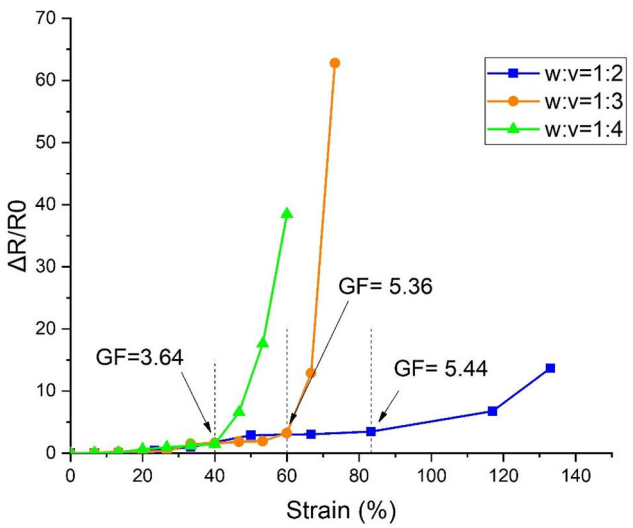


**Fig. 8** Response of strain sensor upon stretching for all ink ratios

detection. The experimental results indicate that as the volume of chitosan solution mixed with the graphite powder increases, the $\Delta R/R_0$ will decrease while the strain detection of the sensor will increase. This can be demonstrated by a significant increase of resistance at strain greater than 80% for strain sensor with ink ratio 1:2. This indicates that the sensor has broken, and the values obtained after the drastic rise are unreliable. The same observation is observed for sensor having ink ratios of 1:3 and 1:4, where a drastic value of $\Delta R/R_0$ occurred at strain greater than 60% and 40%, respectively. This result stipulates that the ability to have the maximum strain withstand and the best stretchability performance is achieved by the strain sensor with ink ratio 1:2 having the maximum attainable strain of 83.3% compared to the ink ratio of 1:3 with 60% and the ink ratio of 1:4 at 40%.

The sensitivity performance of strain sensor is determined by calculating its gauge factor (GF). Figure 9 depicts the changes in GF with respect to attainable strain detection for all three ink ratios. According to the results, the lower the volume of chitosan solution ink mixed with the graphite powder, the higher the sensitivity performance of the strain sensor. For graphite/chitosan ink ratio 1:2, it can be seen that the GF increases linearly starting from 20% strain. However, for the graphite/chitosan ink ratios 1:3 and 1:4, the GF increases non-linearly from 20% strain. This is because the composition of chitosan used in ink ratio 1:2 is sufficient enough to bind the graphite flakes together while excessive volume of chitosan solution used in the other two ink ratios influenced the graphite distribution of the ink. This is in line with the SEM characterization of the three ink ratios discussed previously where the composition of the chitosan solution influenced the morphology of the ink structure, affecting the sensitivity of the strain sensor for each ink ratio.

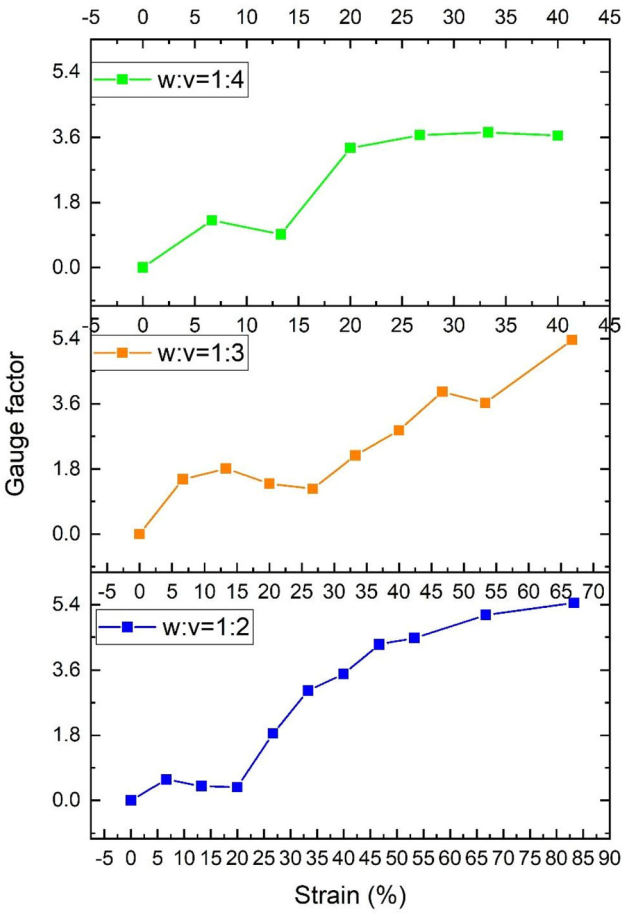


**Fig. 9** Changes of gauge factor with respect to strain for different graphite/chitosan ink ratios

Figure 10 shows the result of three graphite/chitosan ink ratios represented by ink ratios of 1:2, 1:3, 1:4 after bent for three times, respectively. It is observed that no cracks are formed for strain sensor with graphite/chitosan ink ratio of 1:2 upon bending. The strain sensor is able to return and maintain to its original shape after been bending and relaxing without notable change. On the other hand, small cracks are observed for strain sensor with ink ratio of 1:3 and severe cracks are then discovered for strain sensor having ink ratio of 1:4. This is because the strain sensor with ratio 1:2 has the most optimum and sufficient volume of chitosan solution to bind the graphite powder together, thus avoiding ink breakage. The increasing volume of chitosan solution for strain sensor with ratios 1:3 and 1:4 will contribute to excessive amount of binder in binding the graphite powder. When the volume of binder exceeds the amount of graphite that it needs to bind, this will lessen the binding effects between chitosan solution and the graphite powder as too much binder is present in the ink. In addition, these results correspond with the SEM result for each of the chitosan–graphite ink ratio. As mentioned in the SEM result discussion, the ink ratio of 1:2 has the highest adhesion as the particles are more compact and closer to each other compared to ink ratios of 1:3 and 1:4. Therefore, the presence of ink breakage upon bending for strain sensor having mixture ratio of 1:2 proves that it has an excellent adhesion than sensor with ratios 1:3 and 1:4.

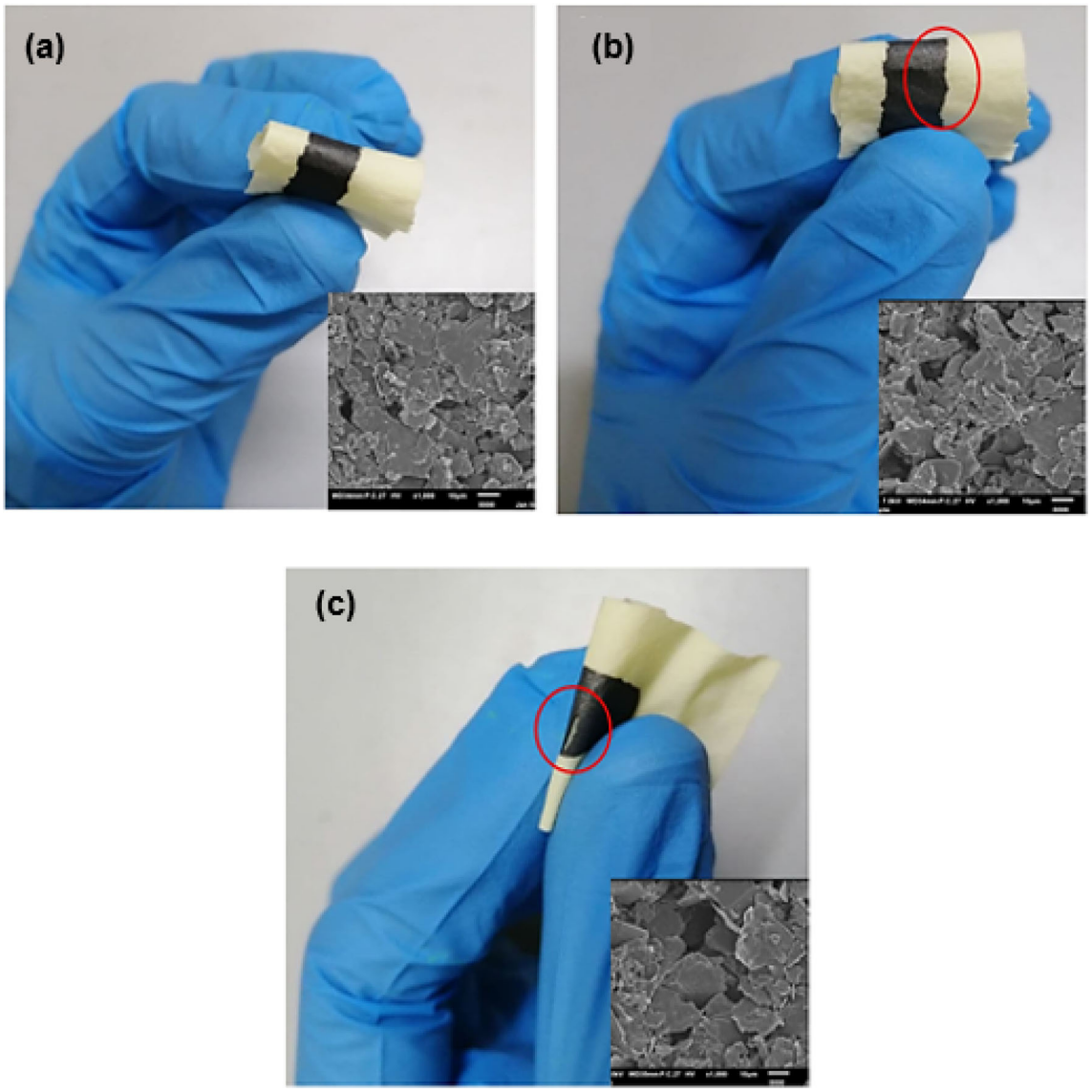


**Fig. 10** Bending test upon strain sensor for all graphite/chitosan ink ratios. **a** Graphite/chitosan ink ratio 1:2. **b** Graphite/chitosan ink ratio 1:3. **c** Graphite/chitosan ink ratio 1:4

Table 1 summarized the performance of all three graphite/chitosan ink ratios of 1:2, 1:3, and 1:4. It can be observed that the performance parameters obtained by graphite/chitosan ink ratio 1:2 are the best. This concluded that the optimum ink ratio to be used is ratio 1:2 compared to 1:3 and 1:4.

Performance of the strain sensor from this work are compared with other previous works as shown in

**Table 1** Performance comparison between the three graphite/chitosan ink ratios

| Graphite/chitosan ink ratio | 1:2 | 1:3 | 1:4 |
|---|---|---|---|
| Resistance obtained | 530 Ω | 550 Ω | 1.6 kΩ |
| Stretchability | 83.3% | 60% | 40% |
| Sensitivity | 5.44 | 5.36 | 3.64 |
| Flexibility (crack upon bending) | No crack observed | Severe crack observed | Severe crack observed |

**Table 2** Comparison of this work with existing chitosan-based strain sensor

| Previous work | 1 (Gong et al. 2015) | 2 (Liu et al. 2017) | This work |
|---|---|---|---|
| Substrate material | Latex rubber | Sponge | Latex glove |
| Active material | Silver nanowires | Carbon black | Graphite powder |
| Binder | Not available | Chitosan | Chitosan |
| Gauge factor | – | 7.5 | 5.45 |
| Measured strain range | 50% | 80% | 83.3% |
| Optimum ink ratio (graphite:chitosan) | – | 1:2 | 1:2 |

Table 2. It can be concluded that the measured strain range detection obtained in this work is higher compared to the benchmark paper strain with 83.3%. The attainable sensitivity in this project does not exceed the previous work, however, the sensitivity obtained is not having big difference from the previous work. Besides, the optimum ratio obtained for this work is in line with the benchmark paper which is the graphite/chitosan ink ratio with ink ratio 1:2.

## 4 Conclusion

In summary, the effect of different graphite/chitosan ink ratios (1:2, 1:3, 1:4) towards the performance of strain sensor were investigated and analyzed. The SEM results show that ink ratio 1:2, having lower volume of chitosan solution, has the most compact structure compared to ink ratios 1:3 and 1:4. As a result, the ink structure of graphite/chitosan 1:2 had the best conductivity and flexibility compared to 1:3 and 1:4. More significantly, the stretchability and sensitivity performance of graphite/chitosan strain sensor ratio 1:2 recorded to be having the best strain detection at 83.3% and GF of 5.44. This result stipulates that ink ratio 1:2 was the optimum ratio to be used. This shows that graphite/chitosan ink is a potential candidate for flexible and stretchable strain sensor as wearable devices in various applications.

## Acknowledgements

This work is fully supported by the Ministry of Higher Education (MOHE) Fundamental Research Grant Scheme (FRGS 21-249-0858) (Grant No: FRGS/1/2021/TK0/UIAM/02/14).

## Author contribution

The authors confirm the contribution as follows: study and idea conception and design: AAMR Synthesis, characterization and measurements: NIIMH Analysis and interpretation of results AAMR, NIIMH, FBA, MAbMH Draft Manuscript preparation: NIIMH in consultation with AAMR, FBA and MAbMH. Supervised the findings of the project: AAMR All authors discussed the results and contributed to the final manuscript, reviewed the results and approved the final version of the manuscript. All authors whose names appear on the submission: made substantial contributions to the conception or design of the work; or the acquisition, analysis, or interpretation of data; or the creation of new software used in the work; drafted the work or revised it critically for important intellectual content; approved the version to be published; and agree to be accountable for all aspects of the work in ensuring that questions related to the accuracy or integrity of any part of the work are appropriately investigated and resolved.

## Funding

This work is fully supported by the Ministry of Higher Education (MOHE) Fundamental Research Grant Scheme (FRGS 21-249-0858) (Grant No: FRGS/1/2021/TK0/UIAM/02/14).

## Data availability

The datasets generated during and/or analyzed during the current study are available from the corresponding author on reasonable request.

## Declarations

**Conflict of interest** The authors declare that they have no known competing financial interests or personal relationships that could have appeared to influence the work reported in this paper.

**Ethical approval** All authors certify that they have no affiliations with or involvement in any organization or entity with any financial interest or non-financial interest in the subject matter or materials discussed in this manuscript.

**Research involving human and animal rights** The authors declare that this research does not contain any studies involving human participants and/or animals.

## References


1. X. Liu et al., Overview of spintronic sensors with internet of things for smart living. IEEE Trans. Magn. (2019). https://doi.org/10.1109/TMAG.2019.2927457
2. A.A. Rifat et al., Photonic crystal fiber based plasmonic sensors. Sens. Actuators B **243**(November), 311–325 (2017). https://doi.org/10.1016/j.snb.2016.11.113
3. J. Ge et al., A stretchable electronic fabric artificial skin with pressure-, lateral strain-, and flexion-sensitive properties. Adv. Mater. **28**(4), 722–728 (2016). https://doi.org/10.1002/adma.201504239
4. T. Yang, D. Xie, Z. Li, H. Zhu, Recent advances in wearable tactile sensors: Materials, sensing mechanisms, and device performance. Mater. Sci. Eng. R **115**, 1–37 (2017). https://doi.org/10.1016/j.mser.2017.02.001
5. K. Senthil Kumar, P.-Y. Chen, H. Ren, A review of printable flexible and stretchable tactile sensors. Research **2019**, 1–32 (2019). https://doi.org/10.34133/2019/3018568
6. Q. Li et al., Engineering of carbon nanotube/polydimethylsiloxane nanocomposites with enhanced sensitivity for wearable motion sensors. J. Mater. Chem. C **5**(42), 11092–11099 (2017). https://doi.org/10.1039/c7tc03434b
7. S. Gong et al., Highly stretchy black gold E-skin nanopatches as highly sensitive wearable biomedical sensors. Adv. Electron. Mater. **1**(4), 1–7 (2015). https://doi.org/10.1002/aelm.201400063
8. W. Tang, T. Yan, J. Ping, J. Wu, Y. Ying, Rapid fabrication of flexible and stretchable strain sensor by chitosan-based water ink for plants growth monitoring. Adv. Mater. Technol. **2**(7), 1–5 (2017). https://doi.org/10.1002/admt.201700021
9. W. Tang et al., Rapid fabrication of wearable carbon nanotube/graphite strain sensor for real-time monitoring of plant growth. Carbon N. Y. **147**, 295–302 (2019). https://doi.org/10.1016/j.carbon.2019.03.002
10. J. Kim, R. Kumar, A.J. Bandodkar, J. Wang, Advanced materials for printed wearable electrochemical devices: a review. Adv. Electron. Mater. **3**(1), 1–15 (2017). https://doi.org/10.1002/aelm.201600260
11. J.Z. Gul, M. Sajid, K.H. Choi, 3D printed highly flexible strain sensor based on TPU-graphene composite for feedback from high speed robotic applications. J. Mater. Chem. C **7**(16), 4692–4701 (2019). https://doi.org/10.1039/c8tc03423k
12. J.J. Park, W.J. Hyun, S.C. Mun, Y.T. Park, O.O. Park, Highly stretchable and wearable graphene strain sensors with controllable sensitivity for human motion monitoring. ACS Appl. Mater. Interfaces **7**(11), 6317–6324 (2015). https://doi.org/10.1021/acsami.5b00695
13. Y. Liu, H. Zheng, M. Liu, High performance strain sensors based on chitosan/carbon black composite sponges. Mater. Des. **141**, 276–285 (2018). https://doi.org/10.1016/j.matdes.2017.12.046
14. C. Mattmann, F. Clemens, G. Tröster, Sensor for measuring strain in textile. Sensors **8**(6), 3719–3732 (2008). https://doi.org/10.3390/s8063719
15. M. Mohammed Ali et al., Printed strain sensor based on silver nanowire/silver flake composite on flexible and stretchable TPU substrate. Sens. Actuators A **274**, 109–115 (2018). https://doi.org/10.1016/j.sna.2018.03.003
16. M. Hu, X. Cai, Q. Guo, B. Bian, T. Zhang, J. Yang, Direct pen writing of adhesive particle-free ultrahigh silver salt-loaded composite ink for stretchable circuits. ACS Nano **10**(1), 396–404 (2016). https://doi.org/10.1021/acsnano.5b05082
17. A.J. Bandodkar, R. Nuñez-Flores, W. Jia, J. Wang, All-printed stretchable electrochemical devices. Adv. Mater. **27**(19), 3060–3065 (2015). https://doi.org/10.1002/adma.201500768
18. R. Ma, B. Kang, S. Cho, M. Choi, S. Baik, Extraordinarily high conductivity of stretchable fibers of polyurethane and silver nanoflowers. ACS Nano **9**(11), 10876–10886 (2015). https://doi.org/10.1021/acsnano.5b03864
19. J.Y. Je, S.K. Kim, *Chitosan as Potential Marine Nutraceutical*, 1st edn. (Elsevier Inc., Amsterdam, 2012)
20. J. Park, I. You, S. Shin, U. Jeong, Material approaches to stretchable strain sensors. ChemPhysChem **16**(6), 1155–1163 (2015). https://doi.org/10.1002/cphc.201402810
21. M. Balyan, T.I. Nasution, I. Nainggolan, H. Mohamad, Z.A. Ahmad, Energy harvesting properties of chitosan film in harvesting water vapour into electrical energy. J. Mater. Sci. Mater. Electron. **30**(17), 16275–16286 (2019). https://doi.org/10.1007/s10854-019-01998-3

22. M.M. Ayad, I.M. Minisy, Detection and kinetics of methylamine on chitosan film coated quartz crystal microbalance electrode. Prog. Org. Coatings **100**, 76–80 (2016). https://doi.org/10.1016/j.porgcoat.2016.01.012
23. M.T. Yen, J.H. Yang, J.L. Mau, Physicochemical characterization of chitin and chitosan from crab shells. Carbohydr. Polym. **75**(1), 15–21 (2009). https://doi.org/10.1016/j.carbpol.2008.06.006
24. E. Chorbadzhiyska, I. Bardarov, Y. Hubenova, M. Mitov, Graphite–metal oxide composites as potential anodic catalysts for microbial fuel cells. Catalysts **10**(7), 1–14 (2020). https://doi.org/10.3390/catal10070796
25. A.H. Gedam, R.S. Dongre, A.K. Bansiwal, Synthesis and characterization of graphite doped chitosan composite for batch adsorption of lead(II) ions from aqueous solution. Adv. Mater. Lett. **6**(1), 59–67 (2015). https://doi.org/10.5185/amlett.2015.7592
26. A.A. Dubale et al., The synergetic effect of graphene on $Cu_2O$ nanowire arrays as a highly efficient hydrogen evolution photocathode in water splitting. J. Mater. Chem. A **2**(43), 18383–18397 (2014). https://doi.org/10.1039/c4ta03464c
27. M. Ali, Raman Characterization of Structural Properties of Thermally Modified Nanographite. vol. Independen, p. 49, 2015